Laser Treatment of Rene-41: Thermal and Microstructural Analysis

B. S. Yilbas
Professor
e-mail: bsyilbas@kfupm.edu.sa

Sohail Akhtar
Assistant Professor
e-mail: ssakhtar@kfupm.edu.sa

Department of Mechanical Engineering,
KFUPM Box 1913,
Dhahran, 31261, Saudi Arabia

C. Karatas
Faculty of Engineering,
Hacettepe University,
Ankara, 06800, Turkey

Laser treatment of Rene 41 surface is carried out at high pressure environment of nitrogen. Temperature and stress fields are predicted using ABAQUS finite element code. Metallurgical and morphological changes in the laser treated layer are examined using optical and scanning electron microscopes (SEM). The residual stress formed at the surface vicinity is obtained by X-ray diffraction (XRD) technique. It is found that the predictions of the residual stress agree well with the results obtained from the XRD technique. Cellular or cellular dendritic structures with fine secondary dendrites are formed in the laser treated surface due to high cooling rates. In addition, γ' particles formed are generally in cubic morphology with varying sizes.
[DOI: 10.1115/1.4024289]

Keywords: laser treatment, Rene 41, microstructure, thermal stress

Introduction

Rene 41 is a precipitation hardened superalloy with a poor processing ductility because of its high cracking tendency at high mechanical forces due to the presence of γ' forming elements. The surface properties of the superalloy can be improved through rapid solidification, since low solidification rate results in coarse dendrite structure. This causes serious interdendritic segregation and solidification defects [1]. On the other hand, high rate of solidification results in finer dendrite arm spacing and reduced elemental segregation. Laser surface laser treatment can be considered as one of the effective methods to modify the alloy surface improving the properties, such as hardness, wear, and corrosion resistances. High cooling rates causes formation of high temperature gradients in the irradiated region while developing excessive thermal stresses in this region. Consequently, investigation into laser surface treatment of Rene 41 and thermal stress development in the treated layer becomes essential. Considerable research studies were carried out to examine laser processing of superalloys [2–8]. However, the previous studies were focused on the microstructural analysis and thermal stress fields were left obscure.

In the present study, laser surface treatment of Rene 41 at high pressure nitrogen gas ambient is carried out. The morphological and microstructural changes in the laser treated layer are examined using optical and scanning electron microscopes. Thermal stress formed in the laser treated surface is simulated using ABAQUS finite element code. The residual stress formed in the surface region is determined incorporating the XRD technique and findings are compared with the predictions.

Contributed by the Manufacturing Engineering Division of ASME for publication in the JOURNAL OF MANUFACTURING SCIENCE AND ENGINEERING. Manuscript received December 25, 2011; final manuscript received April 4, 2013; published online May 27, 2013. Assoc. Editor: Wei Li.

Table 1 Properties used in the simulations. The Poisson's ratio (υ) is 0.32, latent heat of melting is 400,000 J/g, solidus temperature is 1589 K, liquidus temperature is 1644 K, and specific heat capacity is 452 J/kg K.

T (K)	300	450	650	850	950	1050	1150
k (W/mK)	10	11.5	14.7	18.9	21.1	23.2	25.2
α $(1/K) \times 10^{-5}$	1.26	1.28	1.3	1.35	1.4	1.48	1.58
E (GPa)	218	214	202	188	179	171	160
Yield limit (GPa)	1.062	1.062	1.055	1.014	1.00	0.938	0.814

Heating and Thermal Stress Analysis

Heat conduction and phase change with temperature-dependent conductivity, internal energy (including latent heat effects), and convection and radiation boundary conditions are considered in

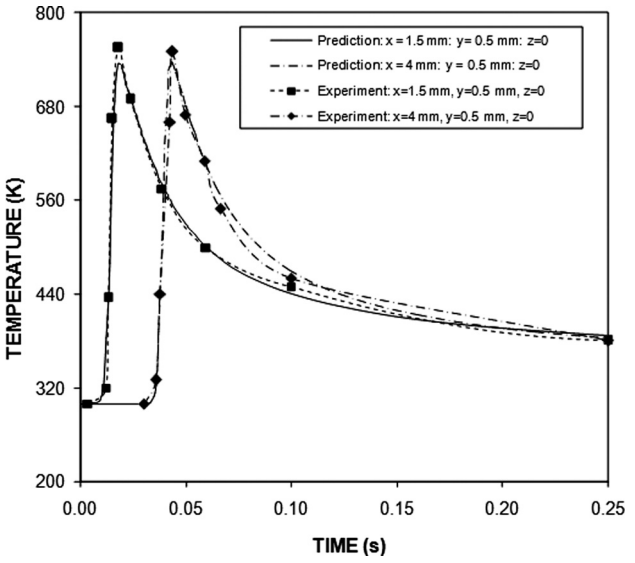

Fig. 1 Thermocouple data and temperature predictions with time

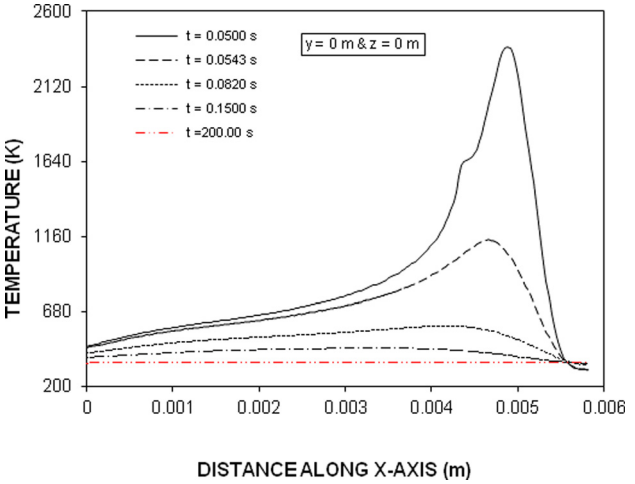

Fig. 2 Temperature variation along the *x*-axis for various cooling periods. The cooling period is started at $t = 0.05$.

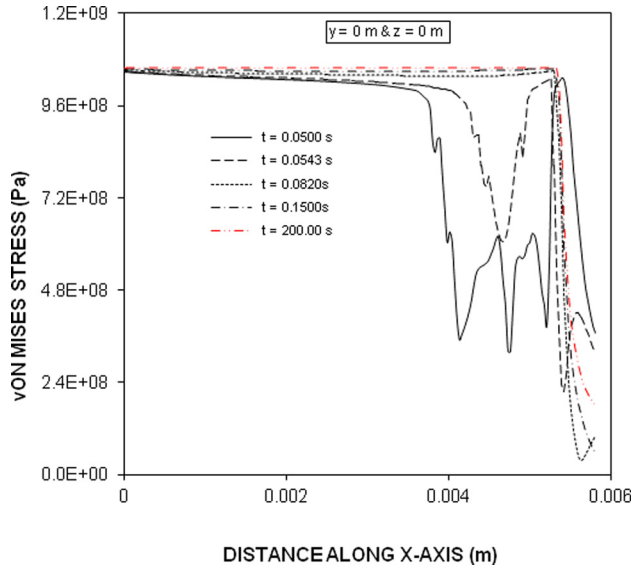

Fig. 3 von Mises stress variation along the *x*-axis for different cooling periods. The cooling period starts at $t = 0.05$ s.

the analysis. The fixed boundary conditions are applied on the both ends of the workpiece resembling the experimental laser heating situation. Laser heat flux with Gauss distribution and prescribed velocity of 10 cm/s along the x-axis through user subroutine DFLUX is applied to the thermal model using the ABAQUS software [9]. The Gauss parameter "a" is $a = 0.0003$ m, in accordance with the experimental power intensity distribution. Cooling was allowed to continue until all of the plate reaches initial temperature (room temperature). The workpiece is considered as an elastoplastic body, which is modeled as von Mises elastic-plastic material with isotropic hardening and with a yield stress that changes with temperature. The phase change is modeled using the variable specific heat capacity [9]. The details of analysis for temperature and stress fields are similar to those given in Ref. [10]. Table 1 gives the properties of Rene used in the simulations [11].

Experimental

The CO_2 laser (LC-ALPHAIII) delivering nominal output power of 2 kW was used to irradiate the workpiece surface. Nitrogen assisting gas coaxially with the laser beam was used. The large range of laser treatment parameters was incorporated in the initial laser treatment tests; the range of parameters resulting in depth of 40 μm laser treated layer and free surface cracks was selected.

Rene 41 sheet plates with 3 mm thickness were prepared at dimensions $15 \times 20 \times 3$ (length $\times$ width $\times$ thickness) mm^3. Jeol 6460 electron microscopy was used for SEM examinations and the Bruker D8 Advance having Cu-Kα ($\lambda = 1.5406$ Å) radiation was used for XRD analysis. The XRD technique is used for the residual measurement measurements. The relationship between the peak shift and the residual stress (σ) is given in the previous study [12]. The (114) reflection from the ε-Fe_3N (interplaner spacing of 0.8570 Å at 128.445 deg) was used for residual stress measurements. The linear dependence of d(114) results in the slope of -4.11×10^{-13} m/deg and the intercept of 0.8570 Å. The residual stress determined from the XRD technique at the surface vicinity is on the order of -720 ± 20 MPa. Measurements are repeated three times and the error related to the measurements is on the order of 3%. The standard test method for Vickers indentation hardness of advanced ceramics (ASTM C1327-99) was adopted and 300 mg load was used during the tests. The measurements were repeated three times at each location at the surface and the error estimated is on the order of 5%.

To validate temperature predictions, two thermocouples were used for surface temperature measurement at the location 0.5 mm away from the laser irradiated spot center to avoid the melting of the surface of the thermocouples. The thermocouples output were calibrated according to the previous study [13]. The experimental error was estimated on the order of 5%.

Results and Discussion

Figure 1 shows temporal variation of thermocouple data and predictions of surface temperature at two locations on the workpiece surface. The predictions of surface temperature are in good agreement with the thermocouple data. The small discrepancies are associated with the assumptions made in the simulations and experimental error, which is on the order of 5%.

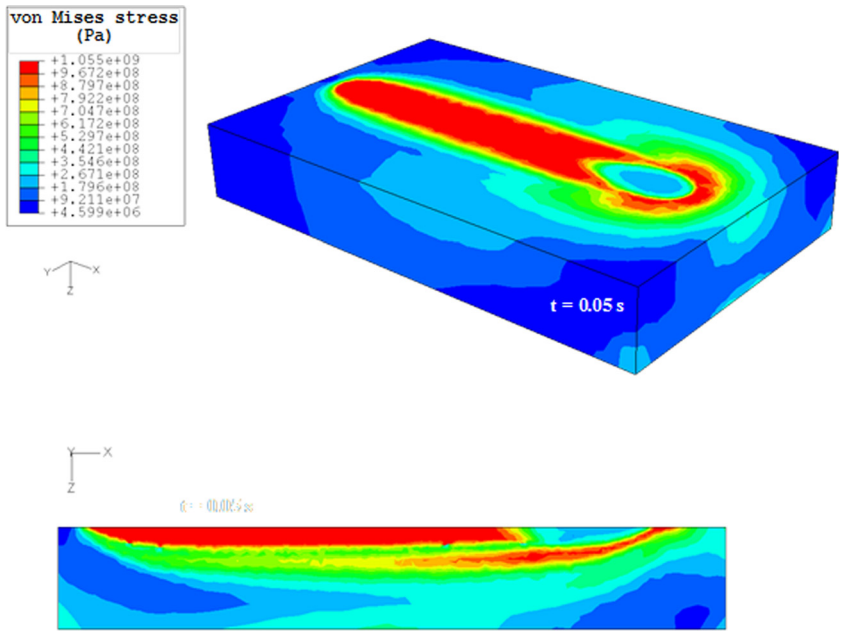

Fig. 4 von Mises stress contours inside the substrate material at the cooling cycle initiation

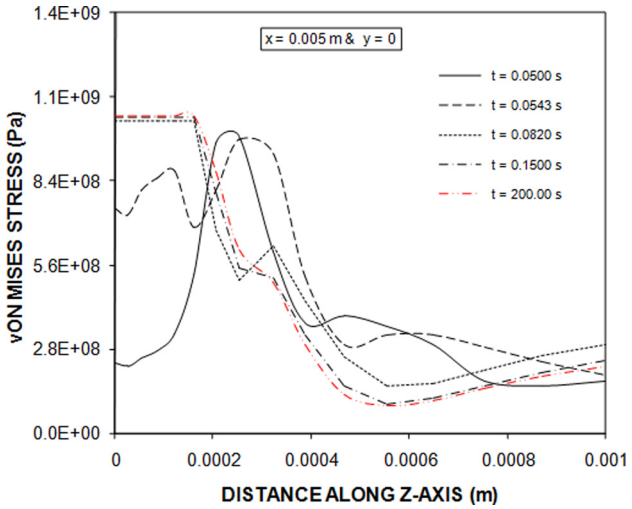

Fig. 5 von Mises stress variation along *z*-axis for different cooling periods. The cooling cycle initiates at $t = 0.05$ s.

Figure 2 shows temperature distribution along the x-axis for different cooling periods. Time $t = 0.05$ s corresponds to the initiation of the cooling cycle. Temperature is maximum at the onset of cooling at location $x = 0.005$ m where the laser power is ceased off. Temperature reaches well above the liquidus temperature of the substrate material at the irradiated spot center. This, in turn, results in superheating of the liquid phase in this region. Since the laser heating is initiated at a location $x = 0$, temperature reduces between $0 \leq x \leq 0.004$ m due to the convection and conduction cooling and the temperature gradient remains low in this region. As the cooling cycle progresses, temperature reduces. The reduction in temperature at the irradiated spot center is larger than that of other locations along the x-axis. This is attributed to the high rate of heat conduction from this region to the solid bulk. As the cooling cycle progresses further, temperature reduces to initial temperature and cooling cycle ends at $t = 200$ s.

Figure 3 shows von Mises stress variation along the x-axis for various cooling periods, while Fig. 4 shows von Mises stress contours in the treated region. von Mises stress attains low values at high temperature because of the temperature dependant elastic modulus which reduces with increasing temperature (Table 1). However, von Mises stress attains high values in the vicinity of irradiated spot center ($x > 0.005$ m) due to the attainment high temperature gradients in this region. As the cooling cycle

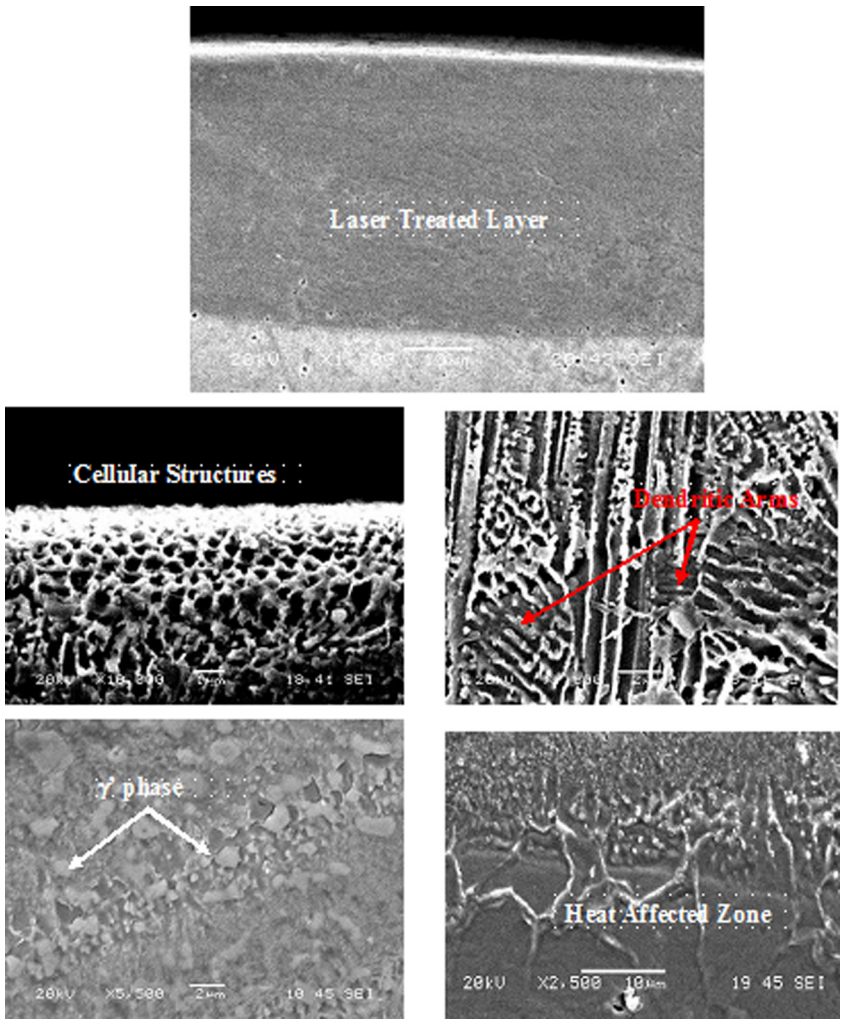

Fig. 6 Cross section of the laser treated surface: (*a*) uniform treated layer with almost 40 μm thickness below the surface, (*b*) fine and dense cellular structures at the surface vicinity, (*c*) dendritic structure and short interdendritic arms, (*d*) γ' phases below the treated surface, and (*e*) large grains at the vicinity of heat affected zone

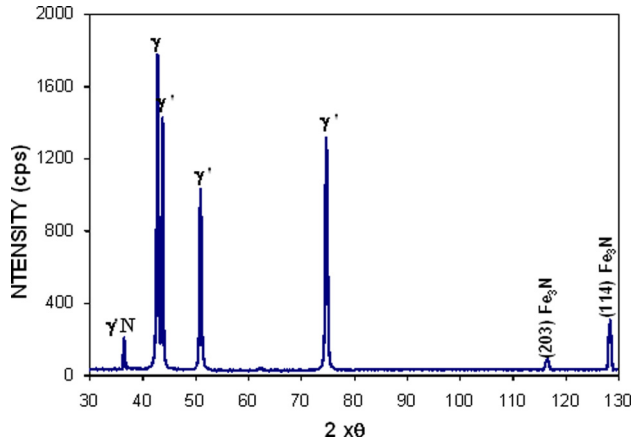

Fig. 7 XRD diffractogram for laser treated surface

progresses, von Mises stress increases in the region where the temperature gradient is initially high. As the cooling cycle progresses further, von Mises stress reaches its maximum in the region $0.004\,\text{m} \leq x \leq 0.0055\,\text{m}$.

Figure 5 shows von Mises stress distribution along the z-axis for different cooling periods. von Mises stress attains low values in the surface region during the early cooling periods ($t \leq 0.543$ s), which is because of high temperature developed in this region. As the cooling cycle progresses further, von Mises stress attains the highest value in the surface vicinity and it remains almost the same toward the cooling cycle ends. The maximum value of von Mises stress is on the order of 1 GPa at the surface region of the substrate material. The predicted residual stress in the surface vicinity is on the order of -680 MPa. Moreover, the residual stress obtained from the XRD measurement is on the order of -720 ± 20 MPa. It is evident that both results are in good agreement. The small difference between the results is associated with the assumptions considered in the simulations, such as homogeneous structures, and the experimental errors, which is about 3%.

Figure 6 shows SEM micrograph of the cross section of the laser treated surface. The uniform laser treated layer with 50 μm thickness is evident from the SEM micrograph. The presence of the demarcation line is attributed to high cooling rates taking place in the laser treated layer. In addition, formation of large grains at the interface region of the base material is evident due to the presence of the heat affected zone. Moreover, the high cooling rates in the surface region resulted in cellular or cellular dendrite structures with some secondary dendrite arms. This is attributed to the high rate of solidification at the surface, which results in epitaxially formed fine and directionally solidified cellular dendrites.

Figure 7 shows XRD diffractogram of the laser treated surface. The presence of γ and γ' phases is evident from the XRD peaks. Formation of γ'N nitride species at the surface is notable. This could be attributed to nitrogen diffusion in the region of the surface vicinity at high temperature during the laser treatment process. The elemental composition of the treated surface does not change during the treatment process as observed from the energy dispersive spectroscopy data. This can be attributed to the formation of γ'N species at the surface. The microhardness of the laser treated surface improves from 390 HV to 460 HV, which is associated with the formation of fine grains and γ'N nitride species at the surface.

Conclusion

Laser treatment of Rene 41 surface is carried out under high nitrogen pressure environment. Temperature and thermal stress fields are simulated using the ABAQUS finite element code. Morphological and metallurgical changes in the laser treated region are examined through optical and scanning electron microscopes. Microhardness of the laser treatment surface is measured and compared with its counterpart obtained for the as received surface. The residual stress developed at the surface vicinity is determined from the XRD technique. It is found that temperature decays sharply in the neighborhood of the irradiated spot center resulting in high temperature gradients in this region, which is more pronounced in the early cooling periods. The self-annealing affect lowers stress levels in low temperature region. von Mises stress reduces in the region of high temperature due to reduced elastic modulus with increasing temperature. The residual stress is compressive and attains high values in the surface region. High cooling rates resulted in cellular or cellular dendrite structures in the surface region. The secondary dendrite formation in the surface vicinity is suppressed by the epiaxially formed cellular dendrites, which is associated with high cooling rates in the surface region. γ' particles are generally in cubic morphology with varying sizes, which is associated with competitive coarsening due to minimization of interfacial energy. Microhardness attains high values for laser treated surface which is associated with fine grains and γ'N species formation at the surface.

Acknowledgment

The authors acknowledge the support of King Fahd University of Petroleum and Minerals Dhahran, Saudi Arabia and Karmetal AS in Turkey for this work.

References

[1] Li, J., and Wang, H. M., 2010, "Microstructure and Mechanical Properties of Rapid Directionally Solidified Ni-Base Superalloy Rene 41 by Laser Melting Deposition Manufacturing," Mater. Sci. Eng., A, **527**, pp. 4823–4829.
[2] Huang, X., Li, Y., Liu, Y., Peng, H., and Azer, M., 2006, "Laser Near Net Shape Manufacturing for Nickel Alloy Parts With Complex Structure," 2nd Pacific International Conference on Applications of Laser and Optics Conference Proceedings (PICALO 2006), pp. 196–200.
[3] Neidel, A., Riesenbeck, S., Ullrich, T., Volker, J., and Yao, C., 2005, "Hot Cracking in the HAZ of Laser-Drilled Turbine Blades Made From René 80," Materialpruefung/Mater. Test., **47**, pp. 553–559.
[4] Kelbassa, I., Walther, K., Trippe, L., Meiners, W., Over, C., and Hangkong, D. X., 2007, "Potentials of Manufacture and Repair of Nickel Base Turbine Components Used in Aero Engines and Power Plants by Laser Metal Deposition and Laser Drilling," J. Aerosp. Power, **22**, pp. 739–748.
[5] Santos, E. C., Kida, K., Carroll, P., and Vilar, R., 2011, "Optimization of Laser Deposited Ni-Based Single Crystal Superalloys Microstructure," Adv. Mater. Res., **154–155**, pp. 1405–1414.
[6] Rush, M. T., Colegrove, P. A., Zhang, Z., and Courtot, B., 2010, "An Investigation Into Cracking in Nickel-Base Superalloy Repair Welds," Adv. Mater. Res., **89–91**, pp. 467–472.
[7] Abdul Aleem, B. J., Hashmi, M. S. J., and Yilbas, B. S., 2011, "Laser Controlled Melting of Pre-Prepared Inconel 718 Alloy Surface," Opt. Lasers Eng., **49**(11), pp. 1314–1319.
[8] Yilbas, B. S., and Akhtar, S., 2011, "Laser Welding of Haynes 188 Alloy Sheet: Thermal Stress Analysis," Int. J. Adv. Manuf. Technol., **56**(1–4), pp. 115–124.
[9] ABAQUS Theory Manual, Version 6.2, ABAQUS, Inc., Pawtucket, RI.
[10] Yilbas, B. S., and Akhtar, S., 2012, "Laser Re-Melting of HVOF Coating With WC Blend: Thermal Stress Analysis," J. Mater. Process. Technol., **212**, pp. 2569–2577.
[11] Rene 41 Technical Data, http://www.hightempmetals.com/techdata/hitempRene41data.php
[12] Khana, Z. A., Hadfield, M., Tobe, S., and Wang, Y., 2005, "Ceramic Rolling Elements With Ring Crack Defects—A Residual Stress Approach," Mater. Sci. Eng., A, **404**, pp. 221–226.
[13] Yilbas, B. S., Davies, R., Gorur, A., Yilbas, Z., Begh, F., Kalkat, M., and Akcakoyun, N., 1990, "Study Into the Measurement and Prediction of Penetration Time During CO_2 Laser Cutting Process," Proc. Inst. Mech. Eng., Part B, **204**, pp.105–113.